Ocean Sci. Discuss., https://doi.org/10.5194/os-2018-119
Manuscript under review for journal Ocean Sci.
Discussion started: 16 November 2018

Ocean Science
Discussions
Open Access
EGU

Synoptic scale variability of surface winds and expected changes in the ocean-atmosphere dynamics of the eastern Austral Pacific Ocean

Iván Pérez-Santos[1, 2], Romanet Seguel[2, 3, 4] and Wolfgang Schneider[5, 6]

[1]Centro i-mar de la Universidad de los Lagos, Puerto Montt, Chile
[2]Centro de Investigación Oceanográfica COPAS Sur-Austral, Universidad de Concepción, Chile
[3]Programa de Postgrado en Oceanografía, Departamento de Oceanografía, Universidad de Concepción, Chile
[4]Instituto de Fomento Pesquero, Aysén, Chile
[5]Departamento de Oceanografía, Campus Concepción, Universidad de Concepción, Chile
[6]Millennium Institute of Oceanography (IMO), University of Concepción, Chile

*Corresponding author: Iván Pérez-Santos: ivan.perez@ulagos.cl

Abstract. In the southern hemisphere, macroscale atmospheric systems such as the westerly winds and the Southeast Pacific Subtropical anti-cyclone (SPSA) influence the wind regime of the eastern Austral Pacific Ocean. The average and seasonal behaviors of these systems are well known, although wind variability at different time and distance scales was previously unexamined. The main goal of this study was, therefore, to determine the space and time scale variabilities of surface winds from 40° to 56° S, using QuikSCAT, ASCAT, and ERA-Interim surface wind information, complemented by in situ meteorological data. In addition, interactions between atmospheric systems, together with the ocean-atmosphere dynamics, were evaluated, from 1999 to 2015. The empirical orthogonal function detected dominance at the synoptic scale in mode 1, representing approximately 30 % of the total variance. In this mode, low and high atmospheric pressure systems characterized wind variability, with a cycle length of 16.5 days. Initially, mode 2, representing approximately 22 % of the variance, was represented by westerly winds (43° to56° S), which occurred mostly during spring and summer, with an annual time scale (1999-2008), until they were replaced by systems cycling at 27.5 days (2008-2015), reflecting the influence of the Southern Hemisphere´s baroclinic annular mode. Mode 3, representing approximately 15 % of the variance, involved passage of small scale, low and high atmospheric pressure (LAP, HAP) systems throughout Patagonia. Persistent Ekman suction south of the Gulf of Penas, and up to and beyond the Pacific mouth of the Magellan Strait, occurred throughout the year. Easterly Ekman transport (ET) piled these upwelled waters onto the western shore of South America, when the winds blew southward. These physical mechanisms were essential in bringing nutrients to the surface, and then transporting planktonic organisms from the oceanic zone into Patagonian fjords and channels. In a variation, between 41° and43° S, surface wind from the SPSA produced offshore ET during spring and summer, causing reduced sea surface temperature, and increased chlorophyll-a; this is the first time that such upwelling conditions have been reported so far south, in the eastern Pacific Ocean. The influence of northward migrating LAP systems on the ocean-atmosphere interphase allowed us to understand, for the first time, their direct relationship with recorded night time air temperature maxima (locally referred to as “Nighttime heat wave events”). In the

Ocean Sci. Discuss., https://doi.org/10.5194/os-2018-119
Manuscript under review for journal Ocean Sci.
Discussion started: 16 November 2018

context of global climate change, greater attention should be paid to these processes, based on their possible impact on the rate of glacier melting, and on the austral climate.

Keywords: Atmospheric pressure systems, Ekman transport, Pacific Ocean, Patagonia, synoptic scale

1. Introduction

The eastern Austral Pacific Ocean (40° to56° S) is under the influence of westerly winds, and the Southeast Pacific Subtropical anti-cyclone (SPSA) (Tomczak and Godfrey, 1994; Stewart, 2002). In this region, westerly winds are stronger than those in the northern hemisphere, on average, and extend in a belt from 40° to 60° S (Talley et al., 2011). The SPSA shows an annual migration, reaching its southern position (~40° to 46° S) in the austral summer, owing to the poleward displacement of the intertropical convergence zone (Rahn and Garreaud, 2013; Ancapichun and Garcés-Vargas, 2015; Schneider et al., 2017). The anti-clockwise rotation of winds from the SPSA generates northerly winds along the coastline of Chile and Peru, contributing to the maintenance of upwelling conditions all year around, giving rise to one of the higher productivity marine ecosystems in the world's oceans (Kampf and Chapman, 2016). The system is well known for the contribution of westerly winds and SPSA to the circulation regimen, e.g., formation of the Humboldt Current system (Thiel et al., 2007; Fuenzalida et al., 2008).

While most studies have focused on SPSA behavior (Rahn and Garreaud, 2013; Ancapichun and Garcés-Vargas, 2015; Schneider et al., 2017), and the effect of the ocean-atmospheric interaction, little is known about the surface wind variability in the eastern Austral Pacific Ocean. Therefore, the principal goal of this study was to determine the space and time variability of the surface winds that extend from 40° S to 56° S, using different satellite wind products, and in situ meteorological information. The interaction between the Austral Pacific surface wind regimen and the SPSA was also taken into account, together with ocean-atmosphere dynamics.

The principal hypotheses of our study were: (1) the passage of synoptic-scale atmospheric events throughout the eastern Austral Pacific Ocean, such as low/high atmospheric pressure (LAP and HAP) systems, dominated the surface wind variations in the study area, instead of the westerly wind, producing northerly or southerly winds. (2) The interaction between synoptic scale atmospheric events, such as the SPSA, with LAP systems, allowed the advection of warm air over Patagonia, creating maximum surface air temperatures at nighttime, especially in fall and winter.

In terms of time-distance scales, atmospheric systems have been categorized as macro-,meso-, and microscale (Orlanski, 1975; Ray, 1986; Holton, 1992). The macroscale definition is divided into planetary and synoptic scales. Winds that impact the globe belong to the planetary scale, such as the westerly and trade winds, and also El Niño (Tomasz, 2014), extending over distances from 1000-40000 km, with time scales of weeks or longer. Synoptic scale systems cover 100-5000 km or so, in a timescale of days to weeks, and include events such as atmospheric pressure systems, like subtropical anti-cyclones and hurricanes. Mesoscale events cover a distance and time scale of 1-100 km, in minutes to hours, and include events such as thunderstorms, tornadoes, and sea/land breezes, while microscale systems cover a range of <1 km, and include events such as turbulence, dust devils and gusts, occurring

Ocean Sci. Discuss., https://doi.org/10.5194/os-2018-119
Manuscript under review for journal Ocean Sci.
Discussion started: 16 November 2018

in seconds to minutes. In this manuscript, we evaluated the oceanic response to synoptic scale atmospheric events, including LAP and HAP systems.

The passage of LAP events throughout Patagonian fjords and channels, such as Puyuhuapi Fjord, creates intense vertical mixing that favors microalgal blooms, increasing primary production during the winter season to reach a magnitude similar to the traditionally productive spring-summer season (Montero et al., 2017). In the case of HAP events, which produce alongshore winds (northward), the contribution to the upwelling conditions (offshore Ekman transport) in the northern part of the eastern Austral Pacific coastline have not been quantified. Similarly, LAP systems also produce alongshore winds, although in the opposite direction (southward), and favor downwelling; the mechanisms and effects of these events are addressed in Sect. 3.2.

In the California upwelling systems (32°-44° N), the contribution of Ekman transport (ET) and Ekman pumping (EP), with upward velocities favoring upwelling and primary production, and downward velocities contributing to downwelling, were quantified using an atmospheric model, finding that EP was more important than ET (Pickett and Paduan, 2003). In the central-northern region of Chile, where only ET has been evaluated previously as the leading contributor to upwelling, (Sobarzo and Djurfeldt, 2004), one study (Bravo et al., 2016) have demonstrated that EP contributed 40-60 % of the total upwelling transport. ET and EP, derived here using surface wind products from the QuikSCAT and ASCAT satellites, were used in this study to quantify the contribution of these processes to the total upwelling, with special attention to the offshore region of Chiloe Island (42°-43.5° S), where northward wind occurs during spring-summer, due to the SPSA influence.

In this manuscript, statistical analysis, such as an empirical orthogonal function (EOF) employing surface wind products from the QuikSCAT and ASCAT satellites, from 1999-2015, allowed the importance of the synoptic scale in the wind variability of the eastern Austral Pacific Ocean to be determined, and highlight the occurrence of LAP and HAP systems, with time scales of days. HAP systems and the SPSA contributed to create conditions suitable for upwelling, in the northern part of the study area (offshore Chiloe Island), causing a drop in the sea surface temperature, and increased chlorophyll-a, while LAP systems moved through, mostly in fall and winter, changing climate conditions during nighttime throughout Patagonia. Our results are presented and discussed in Sect.3 and Sect. 4, respectively.

2. Materials and methods

2.1 Satellite surface wind data

Surface wind data was obtained from SeaWinds scatterometers, mounted on the QuikSCAT and ASCAT satellites. QuikSCAT wind vectors were obtained daily, for a 0.5° × 0.5° grid (http://www.ifremer.fr). The root mean square errors (RMSE) for wind velocity and direction were specified to be less than 1.9 m s^{-1} and 17°, respectively (Piolle and Bentamy, 2002). Analysis of QuikSCAT satellite wind data covered the period from July 1999 to November 2009. For the ASCAT wind product, the temporal resolution was also daily-averaged, and the spatial resolution was 0.25° × 0.25°. Comparison of ASCAT wind fields with data from moored buoys showed correlation coefficients of

Ocean Sci. Discuss., https://doi.org/10.5194/os-2018-119
Manuscript under review for journal Ocean Sci.
Discussion started: 16 November 2018

0.86, and the RMSE was less than 2 m s^{-1} (Bentamy and Croize-Fillon, 2011). This product covered the period from April 2007 to December 2015.

ERA-interim product was also used, to understand the origin and influence of the "Nighttime heat wave events" in Patagonia. ERA-interim offer data for surface winds (10 m), air temperature (2 m), and surface atmospheric pressure, with hourly temporal resolution available at 6 hour intervals (0:00, 06:00, 12:00 and 18:00), in a regular grid of 0.75° × 0.75° (Dee et al., 2011).

2.2 Environmental data from buoys and meteorological stations

Data from an oceanographic buoy installed in the northern section of Puyuhuapi Fjord (44° 35.3' S, 72° 43.6' W), and equipped with atmospheric (wind speed and direction, air temperature, and atmospheric pressure), and surface water (temperature and conductivity) sensors, was used to understand fjord-atmosphere interactions. The meteorological data were collected with a temporal resolution of three min, and the water data were registered hourly at ~1 m depth. The time series from the oceanographic buoy started in April 2011 and finished in July 2013. A meteorological station was installed on the coast ~500 m from the buoy, to continue atmospheric measurements in this region. The meteorological station registered atmospheric data every 15 min (wind speed and direction, air temperature, and atmospheric pressure) from April 2014 to August 2017. The atmospheric data from the buoy and meteorological stations were hourly average.

2.3 Sea surface temperature and chlorophyll-a from satellite

Satellite-derived images of chlorophyll-a (chl-a) concentration and sea surface temperature (SST) were obtained from the Moderate Resolution Imaging Spectroradiometer (MODIS) sensor, onboard the Aqua satellite; the data were obtained with a spatial resolution of 4 km^2 per pixel, at nadir, over cloud-free ocean areas, and with a temporal resolution of 8 days. Chl-a and SST images were extracted from the Geospatial Interactive Online Visualization and Analysis Infrastructure (Giovanni; https://giovanni.gsfc.nasa.gov), and were used as evidence of the marine response to the surface winds, and the associated processes, e.g., ET and EP.

2.4 Derived variables

Using QuikSCAT and ASCAT surface wind data, the components of the zonal and meridional wind stress (τ_u and τ_v, respectively), were calculated, as shown in Eq. (1).

$$\tau_u = \rho_a C_d u U_{10},\ \tau_v = \rho_a C_d v U_{10} \quad (1)$$

In Eq. (1), ρ_a is air density (1.2 kg m^{-3}), C_d is a dimension less drag coefficient, u and v are the zonal and meridional wind components, respectively, and U_{10} is the magnitude of the wind vector 10 m above sea level. C_d was calculated using the formula proposed by Yelland and Taylor (1996), in which the coefficient varies as a function of the wind velocity, according to Eq. (2), and Eq. (3).

Ocean Sci. Discuss., https://doi.org/10.5194/os-2018-119
Manuscript under review for journal Ocean Sci.
Discussion started: 16 November 2018

$$C_d = 0.29 + \frac{3.1}{U_{10}} + \frac{7.7}{U^2{}_{10}} \times 10^{-3}, \text{ for } U_{10} \le 6ms^{-1} \quad (2)$$

$$C_d = 0.60 + 0.070U_{10} \times 10^{-3}, \text{ for } 6ms^{-1} \le U_{10} \le 26ms^{-1} \quad (3)$$

Ekman surface transport, M (m^2 s^{-1}), was calculated for each grid point of the satellite wind field using Eq. (4) (Smith, 1968).

$$\bar{M} = \frac{\vec{\tau}}{\rho_w f} \quad (4)$$

In Eq. (4), $\vec{\tau}$ is the wind stress vector, ρ_w is the water density (1025 kg m^{-3}), and f is the Coriolis parameter; the EP velocity, W_E (m^3 s^{-1}), was calculated according to Eq. (5) (Smith, 1968).

$$W_E = \frac{1}{\rho_w f} \nabla \times \vec{\tau} \quad (5)$$

In Eq. (5), $\nabla \times \vec{\tau}$ is the wind stress curl, which was derived by first order cross-differencing of the wind stress field, which implies that no curl computation was possible for the grid points nearest to the coast. This drawback was overcome by applying coKriging, in two dimensions, to the wind stress curl, which allowed extrapolation toward the coast (Marcotte, 1991).

In order to quantify the relative importance of EP to total upwelling transport, EP velocities were integrated up to ~50 km offshore, along three transects, which were located in the northern (42.2° S), central (47.2° S), and southern (52.2° S) parts of the study region (Fig. 5 (a),black dots). The objective of this calculation was to obtain the vertical transport (m^3 s^{-1}) for each selected transect, and compare it with the ET obtained by Eq. (4), following the methodology proposed by Pickett and Paduan (2003).

2.5 Data analysis

Zonal and meridional surface winds from QuikSCAT (1999-2009), and ASCAT (2007-2015), were used to apply a standard empirical orthogonal function (EOF) analysis (Emery and Thomson, 1998; Kaihatu et al., 1998), in order to determine the modes of variability that dominated the spatiotemporal behavior of the wind field in the eastern Austral Pacific Ocean. Before computing the EOFs, long term means and linear trends were removed. This method enabled a more compact description of the spatiotemporal variability of wind, such that the total variability could be grouped into empirical modes, with most of the variability appearing in the first mode.

A Morlet wavelet analysis was applied (Torrence and Compo, 1998) to the time-dependent coefficients of the three modes, resulting from real-vector EOF analysis of the QuikSCAT and ASCAT wind fields. This wavelet analysis allowed distinction of the time and duration of the dominant periods of the different atmospheric processes. The wavelet spectra were used to calculate time-averaged spectra for the entire sampling period, and these are referred to from here on as the global wavelet spectrum (Torrence and Compo, 1998).

Ocean Sci. Discuss., https://doi.org/10.5194/os-2018-119
Manuscript under review for journal Ocean Sci.
Discussion started: 16 November 2018

The statistical moments (hourly, daily, monthly, means and standard deviations) used in our calculations were always estimated employing values from QuikSCAT, ASCAT, and the buoy and meteorological station databases. Before calculating long-term daily and monthly means for the ET and EP presented in Fig. 6, the period of overlap of the surface winds, from QuikSCAT and ASCAT (2007-2009), was analyzed. Three time series from QuikSCAT and ASCAT surface winds were extracted, close to the 42.2° S (northern), 47.2° S (central), and 52.2° S (southern) aspects of the study area. The statistical moment of the overlapping period for the zonal and meridional winds, in the three time series, was R^2~0.7, with a lag=0. This was deemed to be acceptable, and so on that basis, a continuous time series was built, using data from QuikSCAT for July 1999-December 2007, and then continuing with data from ASCAT from January 2008-December 2015.

3. Results

3.1 Surface wind features and variability

Analysis of the surface wind long term daily mean, for the period 1999-2015, using the QuikSCAT and ASCAT satellite products, showed similar patterns (Fig. 1). In general, westerlies were the predominant the surface winds, especially between 42° and 45° S, although a more detailed analysis indicated different features. 1) North of 42° S, the wind was slightly west-southwesterly. 2) South to the 45° S, the wind started an inclination from the west to the northwest direction, and 3) between the 54° S and 56° S, the wind blew along the Austral coast of the Magellan region, while in the rest of the study area, the wind direction was perpendicular to the coast. The surface wind average registered as a meridional gradient, in which low speeds (5-6 m s^{-1}) were observed in the northern domain, and stronger wind (10-12 m s^{-1}) was registered down towards 51° S. The standard deviations were very similar between satellite products (±3.0 to ±4.2 m s^{-1}), representing the same meridional gradient observed in the surface wind magnitude, but the ASCAT data registered lower variability and less intense surface wind magnitude, compared with QuikSCAT (Fig. 1a and Fig. 1b). Computation of the seasonal cycle, using both the QuikSCAT and ASCAT datasets, showed a similar meridional gradient to that obtained in the average analysis, representing the time-persistence and high intensity of the northwesterly winds in the open ocean water of the Magellan region (51° to 56° S).

EOF analysis allowed understanding of the surface wind variability modes, and the distribution of the total variance. The EOF for the QuikSCAT daily data showed concentration of ~70 % of the total variance in the first three empirical modes: EOF-1=30.01 %; EOF-2=22.5 %; EOF-3=16.4 %. For the equivalent ASCAT daily wind data, the EOF represented ~65 % of the total variance, in the first three empirical modes: EOF-1=27.9 %; EOF-2=22.5 %; EOF-3=15.3 %. The spatial structure for the first three modes from the QuikSCAT and ASCAT databases were similar (Fig. 2). In the case of the spatial structure of mode 1 (Fig. 2a and 2d), southerly and southwesterly winds dominated the study area, when the time-dependent coefficient was positive (Fig. 3a and 3j, PC-1). When PC-1 (principal component) was negative, the spatial structure of mode 1 rotated 180°, and northerly and northeasterly winds occurred.

Ocean Sci. Discuss., https://doi.org/10.5194/os-2018-119
Manuscript under review for journal Ocean Sci.
Discussion started: 16 November 2018

The global spectrum analysis carried out for PC-1 denoted the dominant, 16.5 days cycle (Fig. 3b and 3k). The PC-1 monthly mean calculation demonstrated that southerly winds occurred mostly during the fall and spring seasons (Fig. 3c and 3l), while northerly winds were more frequent during winter, spring and summer (Fig. 3c and 3l). The southerly and northerly winds were associated with passage of intense HAP (Fig. 4a), and LAP (Fig. 4b) systems, throughout the study region.

The spatial structure of mode 2 highlights the presence of the easterly (positive time-dependent coefficient), and westerly winds (negative time-dependent coefficient) (Fig. 2b and 2e). The global spectrum for the PC-2 (Fig. 3d and 3e) represented the dominance of the annual cycle of 374 days for the QuikSCAT database. The low pass filtered time series for the PC-2 (Fig. 3d, red line) showed the occurrence of the most positive values during the fall and winter season, represented by the easterly winds (Fig. 3f). The negative part of the PC-2 was observed during spring and summer, highlighting the presence of the westerly winds (Fig. 3f). Even though the spatial structure of mode 2 from the ASCAT database presented a similar pattern to the QuikSCAT mode 2, the annual cycle period was not detected in the spectrum of PC-2 (Fig. 3m and 3n). In this analysis, cycles of 27.5 days and 16.5 days were obtained. The monthly mean for PC-2 coincided with the results from QuikSCAT during winter (easterly winds), and spring (westerly winds), but was different in summer and fall, where the wind direction varied (Fig. 3o). Figs 4c and 4d showed examples of the atmospheric systems involved in the wind direction variability presented in this mode.

The spatial structure of mode 3 represented a clockwise atmospheric circulation (e.g., Fig. 4e) of surface winds, in the same direction as an LAP system, when the time-dependent coefficient was positive (Fig. 2c and 2f). The rotation of the winds became counterclockwise (e.g., Fig. 4f) when the time-dependent coefficient was negative, representing a structure similar to that seen for an HAP system (Fig. 3g and 3p). Periods of 2-8 days were detected in the spectrum analysis of both data sets (QuikSCAT and ASCAT), while semiannual (157 days) and annual cycles were observed in the QuikSCAT and ASCAT winds, respectively (Fig. 3h, 3i, 3q, and 3r).

Wavelet analysis allowed observation of the year-round dominance of the synoptic time scale obtained by PC-1 (Fig. 5a and Fig. 5b). An evident change of time scales was observed for PC-2, e.g., the annual cycle dominated from 2000-2008 (Fig. 5c), but from 2009-2015, a 20 to 30 day cycle was more intense than the annual cycle (Fig. 5d). In PC-3, the semiannual signal observed in the global spectrum (Fig. 4h) occurred during 2004 (Fig. 5e), but while the annual cycle registered in Fig. 4q, was clear in 2011 (Fig. 5f), synoptic time scales were persistent from 2000-2015 (Fig. 5e and Fig. 5f).

3.2 Derived parameters from surface winds and ocean implications

The average dominance of the westerly surface wind stress generally produced a northerly ET in the study region (Fig. 6a and Fig. 6b). On average, the ET ran parallel to the coast, between 41° and 47° S, while from there to 56° S, the inclination of the coastline, and the influence of the westerly wind stress, contributed to change the ET direction to be mostly perpendicular to the coast. This was the region (48° to 56° S), where the highest ET value (2.16 $m^2 s^{-1}$) was recorded, due to the presence of the most intense winds, regionally (Fig. 1). Moreover, a wide area of positive (upward motion), and maximum EP (0.25 m day^{-1}), was observed around 51° S, in the QuikSCAT data, in which

Ocean Sci. Discuss., https://doi.org/10.5194/os-2018-119
Manuscript under review for journal Ocean Sci.
Discussion started: 16 November 2018

positive EP extended across the study area (Fig. 5a).The same area of positive and intense EP was observed in the ASCAT database, although in the northern part of the study region, between 41° and 48° S, the upward EP was located closer to the coast, covering approximately the first ~100 km (Fig. 6b).

In order to understand the annual variability of the ET and EP, and the contribution of both processes to the total upwelling transport (TUT), three data time series were extracted, for the northern, central and southern part of the study region, covering the period 2000-2015 (Fig. 7). In the northern part of the study region, in ocean water west as far as the coast of Chiloe Island, the long term TUT daily mean showed high variability (±0.32 $m^3 s^{-1}$) all year round, and especially during fall and winter, when onshore ET dominated the TUT. This condition changed during spring and summer to show dominance by the offshore ET, but with a weaker magnitude than that for winter. The EP was positive, but contributed less to the TUT (Fig. 7a). The long term, monthly mean of these time series' showed the dominance of downwelling conditions, from April to September (Austral fall-winter). The upwelling started in October and finished in February, with a significant contribution by the ET (Fig. 7b). The cumulative transport was in general favorable to downwelling, from April to December, and showed less upwelling in summer (Fig. 7c).

In the time series for the Gulf of Penas, the all year round variability of the long term daily TUT mean continued (±0.35 $m^3 s^{-1}$), but the offshore ET events decreased, and EP was more negative (Fig. 7d). Downwelling conditions prevailed, due to the dominance of the ET during the year (Fig. 7e), and the cumulative transport was negative (downwelling) for all variables (ET, EP, and TUT), and was higher than in the northern time series (Fig. 7f).

In the southern part of the study region, close to the entrance of the Magellan Strait, the absolute maximum (-2.14 $m^3 s^{-1}$) was reported, along with higher variability of the TUT (±0.41 $m^3 s^{-1}$), which was again dominated by the ET. The EP was positive and favorable for upwelling, but less intense than for the ET (Fig. 7 h). The long term monthly mean for transport showed the highest values for the ET, and the highest contribution of this process to the TUT, even though the EP was positive and favorable for upwelling (Fig. 7i). The cumulative transport was also the most important, compared with the other time series (Fig. 7j).

In general, downwelling conditions dominated the study region, but in the open ocean water around Chiloe Island, upwelling was observed during spring-summer. Using the ASCAT surface wind data, some examples of the derived ET and EP from January were extracted, to evaluate the oceanic response during the favorable upwelling conditions (Fig. 8). The ET and EP were very strong; favoring upwelling along the coast, due to the dominance of southern winds produced by the influence of the SPSA systems (Fig. 8a, 8d, and 8g). The magnitude of EP reached ~3 m d^{-1} during January 10, 2014 (Fig. 8g), and the ET varied from 1.5-3 $m^2 s^{-1}$ in the three examples (Fig. 8a, 8 d, and 8g). The images of sea surface temperature (Fig. 8b, 8e) and 8h) and chlorophyll-a (Fig. 8c, 8f and 8i) obtained during the upwelling, were evidence of the oceanic response to the ET and EP. Along the west coast of Chiloe Island, the sea surface temperature dropped ~4° C, and the chlorophyll-a increased ~10-15 mg m^{-3}, compared with the values showed in the open Pacific Ocean waters. These examples demonstrated the importance of ET and EP in the oceanic response to the wind.

Ocean Sci. Discuss., https://doi.org/10.5194/os-2018-119
Manuscript under review for journal Ocean Sci.
Discussion started: 16 November 2018

3.3 Relationship of synoptic events with nighttime heat waves

During field work in Puyuhuapi Fjord (44.5° S), a maximum surface air temperature (SAT) was recorded at night, coincident with an LAP system moved through the fjord. These observations motivated research into the influence of synoptic events on Patagonian weather conditions. The long term hourly mean SATs, from buoy and meteorological station data, showed the same patterns, with a markedly diurnal cycle, in which the SAT maximum was registered in the afternoon (15:00-18:00, local time), while absolute minima were observed early in the morning (6:00-8:00) (Fig. 9a and Fig. 9b). The observed SAT diurnal cycle responded to solar radiation, as shown in the net solar radiation time series from the buoy and meteorological station (Fig. 9c and Fig. 9d). The histogram of SAT absolute maxima demonstrated a bimodal structure, with a first peak in the afternoon, as was observed in the diurnal cycle (Fig. 9a and Fig. 9b), and a second peak at night, from ~21:00 to 05:00 (Fig. 9e and Fig. 9f). The first peak has already been discussed above, and the balance of this subsection describes investigation of the processes involved in the SAT nighttime maximum, known as "nighttime heat wave events."

Nighttime heat wave events were registered all year round, and 456 such events were recorded over the period 2011-2017 (Fig. 10a). The temperature range from these events was 4 to 20° C, with temperatures between 10° C and 12° C the most common (Fig. 10b). The monthly histogram of the nighttime heat wave events showed most occurrences in fall and winter, with fewer incidences in summer (Fig. 10c). Figure 11 presents an example of this event, which occurred during fall 2011, as shown in the atmospheric data from the oceanographic buoy installed in Puyuhuapi Fjord. The maximum SAT was observed on April 21, 2011, at midnight (00:00, local time), coinciding with a decreased atmospheric pressure, and increased surface wind intensity (Fig. 11a).

In order to explore the causes involved in the augmented air temperature, ERA-interim products were used (Fig. 11b – 11g). Before the event, images from surface wind and atmospheric pressure showed the predominance of a westerly wind, from 45° - 56° S, and northerlies from 30°-35° S (Fig. 11b). At the same time, the SAT showed a meridional gradient, in which high air temperature covered the northern domain of the image (30°-40° S) (Fig. 11c). At midnight on July 21, 2011 (00:00, local time), an LAP system arrived in the eastern Austral Pacific Ocean water, and moved northward, interacting with the southern edge of an SPSA system. LAP systems rotate clockwise, with intense winds of ~25 m s^{-1}, and a minimum atmospheric pressure of 958 mbar (Fig. 11d). The west and northwest winds from the LAP advected southward the maximum air temperature, located north of 40° S, contributing to the increased air temperature and heat in Patagonia, as shown in Fig. 11a. High air temperature due to the LAP winds reached the southern part of Patagonia, close to the Magellan Strait (Fig. 11e). Atmospheric conditions returned to normal days after the LAP passage, (Fig. 11f and Fig. 11g) as shown in Fig. 11b and 11c.

A second example, using atmospheric data from the winter of 2012, demonstrated the increased SAT over Patagonia due to the LAP system influence better (Fig. 12). In this case, the maximum air temperature was again registered when the intensity of the wind increased and atmospheric pressure was low (Fig. 12a). Before this event, winds were from the north and northwest, but less intense, and the high air temperature presented the usual meridional gradient (Fig. 12b and Fig. 12c). At midnight of July 18, 2012, an LAP system entered the study area, and advected high air temperature from the subtropical area southward, to Patagonia. During this nighttime heat wave event, warm air was

Ocean Sci. Discuss., https://doi.org/10.5194/os-2018-119
Manuscript under review for journal Ocean Sci.
Discussion started: 16 November 2018

transported along the coast of Patagonia to ~56° S (Fig. 12d and Fig. 12e). Pre-event atmospheric conditions were restored one day after the passage of the LAP system (Fig. 12f and Fig. 12g).

4. Discussion

The combination of QuikSCAT, ASCAT and ERA-interim satellite wind products, together with in situ measurements of winds from oceanographic buoys and meteorological stations, has facilitated understanding of surface wind variability in the eastern austral Pacific Ocean, and the Patagonian interior. Surface winds were generally westerlies (Fig. 1), and the synoptic scale dominated wind variability, due to the influence of the low/high atmospheric pressure systems, with winds from the northerly /southerly directions, respectively (Fig. 2 and Fig. 3). Implications of the synoptic scale events on the atmosphere-ocean interaction is the focus of this section of the manuscript, owing to the importance of winds to the oceanic responses, such as ET and EP, and their influence on the Patagonian climate.

4.1 Surface wind variability

Satellite data on the long term surface wind daily means, over the period 1999-2015, demonstrated that between 42° - 45° S, the normal wind was perpendicular to the coast, and blew from the west. From 45° S and to 56° S, the predominant wind direction changed to the northwest, reaching its highest intensity in the Magellan region, where it blew parallel to the coast. At the other end of the study region (41°-42° S), the predominant wind was from the southwest, although the intensity was less than in the Magellan region (Fig. 1). To date, the wind regime for this region has only been presented as a conceptual model, to show the influence of the westerlies on the westerly drift current (Thiel et al., 2007; Arkhipkin et al., 2009; KilianandLamy, 2012), and to present the general atmospheric circulation applicable to the west coast of South America (Rahn and Garreaud, 2013; Talley et al., 2011). Even though a map similar to Fig. 1 was presented in Aguirre et al. (2012), using QuikSCAT data (2000-2007), details of the surface wind behavior could not be determined. In addition, winds regime studies, which included derived variables such as EP and ET, focused on the central and northern region of the Chilean and Peruvian coasts, north of 40° S, and had as their main goals explanation of the dynamic of the Southeast Pacific Subtropical anti-cyclone (SPSA), and improved understanding of the wind's influence on this circulation regime (Ancapichun and Garcés-Vargas, 2015; Bravo et al., 2016; Fuenzalida et al., 2008; Schneider et al., 2017).

EOF analysis detected the westerly wind pattern in mode 2 with 22% of the total variance. This wind occurred mainly during spring-summer, before veering to an easterly wind for fall to winter (Fig. 2 and Fig. 3). During the first period of wind analysis (1999-2009), an annual cycle dominated mode 2, but in the second period (2009-2015), this dominance reduced, and cycle periods of 27.5 days and 16.5 days were observed (Fig. 5). The period of 16.5 days denoted the importance of the synoptic time scale, while the 27.5 day cycle suggested the influence of the recently reported Southern Hemisphere´s baroclinic annular mode (BAM), which has been described as displaying an energy band lasting between 20 and 30 days (Thompson and Barnes, 2014; Thompson and Woodworth, 2014). BAM influence was observed by Ross et al., (2015) in a Patagonian fjord (47.8° S), using Acoustic Doppler current

Ocean Sci. Discuss., https://doi.org/10.5194/os-2018-119
Manuscript under review for journal Ocean Sci.
Discussion started: 16 November 2018

profiler (ADCP) data, combined with in situ surface wind and atmospheric pressure records, highlighting the contribution of this atmospheric phenomenon to the intensification and frequency of the LAP systems that occur throughout the Patagonian.

LAP and HAP systems dominated mode 1 of the EOF, contributing ~30 % of the total variance (Fig. 2, 3 and 4). In this mode, southerlies related to the passage of HAP systems, and northerlies produced by LAP systems (Fig. 4), occurred in a time scale of 16.5 days (Fig. 3 and Fig. 5). This illustrated the variability of surface winds in the eastern Austral Pacific Ocean, complementing the westerly winds which have been seen to dominate the wind regime, in average and seasonal data.

In the Yucatan basin and the Caribbean Sea, where trade winds dominate the wind regime, synoptic-scale atmospheric events also dominate mode 1 of the EOF, characterized by the influence of continental cold front systems during fall and winter, and extratropical LAP systems in spring and summer (Pérez-Santos et al., 2010). In the tropical Indian Ocean, EOF analysis also improved understanding of wind variability induced by different phases of the monsoon (Alvarinho et al., 2006). It was also seen that the spatial structure of mode 3 of the EOF indicated passage of other types of LAP and HAP systems, this time covering small areas, as in mode 1, although with a different time scale (Fig. 3 and Fig. 4). In general, surface wind variability in the eastern Austral Pacific Ocean was dominated by synoptic-scale events, in which pressure systems with different distance and time scales played an essential role in the region's wind regime.

4.2 Atmospheric-ocean interactions

The long term ET mean showed that this movement ran parallel to the coast from between 41°and 48° S, and then from 48° S to 58° S, it ran perpendicular (onshore) to the coastline, showing higher magnitude in the Magellan region (Fig. 6). Studies have shown that when onshore ET occurred, downwelling conditions prevailed, and particulates were transported to the coast (Stewart, 2002), favoring the retention of eggs and larvae in the coastal zone (Epifanio and Garvine, 2001; Garland et al., 2002). It has also been shown that when offshore ET occurred, upwelling processes dominated along the coastline, favoring primary production (Escribano et al., 2016; Iriarte et al., 2012; Montero et al., 2007). As argued in the previous section, synoptic scale atmospheric events, such as LAP and HAP systems, dominated wind variability within the study area, especially in its northern domain, where the southern edge of the SPSA arrived during spring-summer. During this time of the year, northerly winds influenced the region, producing offshore ET, as shown by the ET time series for the northern (42.2° S) part of the study area (Fig. 7). Then, the upwelling process occurred along the coastline of Chiloe Island, as was demonstrated by the increased chlorophyll-a and the drop of SST in the area of wind influence (Fig. 8). In addition, EP velocity was positively helping the upward movement of oceanic water, which enhanced the injection of nutrients into the surface layer (Rykaczewski and Checkley, 2008).

To date, coastal upwelling has been reported down as far as the central coastal region of Chile (~36° S) (Sobarzo and Djurfeldt, 2004; Sobarzo et al., 2007), but our work has shown that coastal upwelling can occur as far south as~44° S. In general, however, downwelling conditions, dominated by onshore ET, were observed in the study area, especially in the south, close to the Magellanic region (Fig. 6 and Fig. 7). We have hypothesized that the irregular

Ocean Sci. Discuss., https://doi.org/10.5194/os-2018-119
Manuscript under review for journal Ocean Sci.
Discussion started: 16 November 2018

orographic from 44° to56° S, where the coast is conformed with many islands and channels, could reduce the possibility for oceanic water to sink at the coastline, allowing the opportunity for it to pass to the interior Patagonian fjords, carrying nutrients, eggs, larvae from many species into these areas, to enhance biological production in the southern Patagonian fjords.

In addition, it was noted that it was not only the ocean that responded to the synoptic scale variability of the surface wind, but that atmospheric conditions were also influenced. Two examples demonstrated the importance of synoptic scale events in modifying climate conditions in the austral region (Fig. 11 and Fig. 12), where LAP systems contribute with the origin of the "Nighttime heat wave events."

A conceptual model was built to explain the source of the nighttime heat wave events (Fig. 13). In this model, two atmospheric pressure systems participated: a permanent high pressure located in the north (SPSA), which transported warm air from the subtropical region (over the 40° S), and a synoptic LAP system, which originated in the south, with cold air from the Polar zone (Fig. 13a). The LAP originated in the Austral-Pacific Ocean, and the system moved northward, with intense winds rotating clockwise. The northward moving LAP stopped when it encountered the southern edge of the SPSA, at approximately 40° S (Fig. 13b). At this moment the stronger west and northwest wind from the LAP pulled in the warm air from the SPSA, and advected its heat southward to Patagonia. These events occur more frequently at nighttime, and their impact on the Patagonian climate depends on the intensity of the LAP system winds, and the heat content of the SPSA.

In the contexts of climate change and variability, any increase or trend of change in these events needs to be taken into account, as mechanisms that could contribute to increased glacial meltwater, and alteration of the austral climate.

5. Conclusions

In our study, satellite wind data were used to understand surface wind variability in the eastern Austral Pacific Ocean, a region dominated generally by strong westerlies, and the SPSA. The empirical orthogonal function demonstrated that, within the study area, mode 1 of wind variability was dominated by synoptic scale influences, due to the effects of low and high atmospheric pressure systems, instead of the planetary scale westerlies detected in mode 2. In general, downwelling conditions prevailed in the study region, owing to onshore Ekman transport, but offshore Ekman transport, and upward Ekman pumping, were observed during spring and summer in the northern domain (~41° to 48° S), contributing to reduced sea surface temperature, and increased chlorophyll-a. The arrival of the southern edge of the SPSA during spring and summer was the main impetus behind the upwelling condition, and this is the first time that this condition was reported so far south. In addition, the SPSA was involved in the origin of nighttime heat waves, acting with LAP systems to produce night time air temperature maxima which exceeded the normal midday maxima caused by solar radiation.

Data availability. All data sets used in this manuscript can be request from the corresponding author.

Author contributions. IPS: designed the experiment, collection and analysis satellite data, and manuscript leader. RS: collection and analysis satellite and in situ data, and manuscript revision. WS: designed the experiment, collection and analysis satellite data, and manuscript revision. All authors contributed to the writing of the manuscript.

Competing interest. The authors declare that they have no conflict of interest.

Acknowledgments

Surface wind data was collected as part of FONDECYT Grants 3120038, and 11140161, by Dr. Iván Pérez-Santos, with assistance from Dr. Wolfgang Schneider's research group. Financial support was also provided by Centro Copas Sur Austral PFB31 and AFB170006. We are grateful to Centro Copas Sur Austral for providing data from its oceanographic buoy and a partial scholarship for Romanet Seguel to complete a Magister in Oceanography at the University of Concepción, Chile. We thank Centro de Investigación en Ecosistemas de la Patagonia (CIEP) for providing meteorological information.

References

Alvarinho J. L., Isoguchi, O., and Kawamura, H.: Characteristic patterns of QuikSCAT-based wind stress and turbulent heat flux in the tropical Indian Ocean, Remote Sensing of Environment, Volume 103, Issue 4, pp 398-407, 2006.

Aguirre, C., Pizarro, Ó., Strub, P. T., Garreaud, R., & Barth, J. A.: Seasonal dynamics of the near-surface alongshore flow off central Chile. Journal of Geophysical Research: Oceans, 117(C1), n/a-n/a. https://doi.org/10.1029/2011JC007379, 2012.

Ancapichun, S. and Garcés-Vargas, J.: Variability of the Southeast Pacific Subtropical Anticyclone and its impact on sea surface temperature off north-central Chile. Ciencias Marinas, 41(1), 1–20. https://doi.org/10.7773/cm.v41i1.2338, 2015.

Arkhipkin, A. I., Schuchert, P. C., and Danyushevsky, L.: Otolith chemistry reveals fine population structure and close affinity to the Pacific and Atlantic oceanic spawning grounds in the migratory southern blue whiting (Micromesistiusaustralisaustralis). Fisheries Research, 96(2–3), 188–194. https://doi.org/10.1016/j.fishres.2008.11.002, 2009.

Bentamy A.andCroize-Fillon, D.: Gridded surface wind fields from Metop/ASCAT measurements. International Journal of Remote Sensing, 33, 1729-1754, 2011.

Bravo, L., Ramos, M., Astudillo, O., Dewitte, B., and Goubanova, K.: Seasonal variability of the Ekman transport and pumping in the upwelling system off central-northern Chile (~30° S) based on a high-resolution atmospheric regional model (WRF). Ocean Science, 12(5), 1049–1065. https://doi.org/10.5194/os-12-1049-2016, 2016.

Dee, D.P., Uppalaa, S.M., Simmonsa, A.J., Berrisforda, P., Polia, P., Kobayashib, S., Andraec, U., Balmasedaa, M.A., Balsamoa, G., Bauera, P., Bechtolda, P., Beljaarsa, A.C.M., van de Bergd, L., Bidlota, J., Bormanna, N., Delsola, C., Dragania, R., Fuentesa, M., Geera, A.J., Haimbergere, L., Healya, S.B., Hersbacha, H., Hólm, E.V., Isaksena, L., Kallberg, P., Kohler, M., Matricardia, M., McNallya, A.P., Monge-Sanzf, B.M., Morcrettea, J.-J., Parkg, B.-K., Peubeya, C., de Rosnaya, P., Tavolatoe, C., Thépaut, J.-N., and Vitarta, F.: The ERA-Interim reanalysis: configuration and performance of the data assimilation system. Quart. J. Roy. Meteorol. Soc.137, 553–597, 2011.

Emery, W. J.and Thomson R. E.: Data analysis methods in physical oceanography, 634 pp, Pergamon Press, Oxford, 1998.

Epifanio, C. E. and Garvine, R. W.: Larval Transport on the Atlantic Continental Shelf of North America: a Review. Estuarine, Coastal and Shelf Science, 52, 51–77, doi:10.1006/ecss.2000.0727, 2001.

Escribano, R., Bustos-Ríos, E., Hidalgo, P., and Morales, C. E.: Non-limiting food conditions for growth and production of the copepod community in a highly productive upwelling zone. Continental Shelf Research, 126, 1–14.https://doi.org/10.1016/J.CSR.2016.07.018, 2016.

Fuenzalida, R., Schneider, W., Garcés-Vargas, J., and Bravo L.: Satellite altimetry data reveal jet-like dynamics of the Humboldt Current, J. Geophys. Res., 113, C07043, doi:10.1029/2007JC004684, 2008.

455 Garland, E. D., Zimmer, C.A., Lentz, S.J.: Larval Distributions in Inner-Shelf Waters: The Roles of Wind-Driven Cross-Shelf Currents and diel Vertical Migrations. Limnology and Oceanography, Vol. 47, No. 3, 803-817, 2002,

Holton, J.: An Introduction to Dynamic Meteorology. Academic Press, San Diego, 511 pp, 1992.

Iriarte, J. L., Vargas, C. A., Tapia, F. J., Bermúdez, R., andUrrutia, R. E.: Primary production and plankton carbon
460 biomass in a river-influenced upwelling area off Concepción, Chile. Progress in Oceanography, 92–95, 97–109. https://doi.org/10.1016/J.POCEAN.2011.07.009 2012.

Kaihatu, J.M., Handler, R.A., Marmorino, G.O., and Shay, L.K.: Empirical Orthogonal Function Analysis of Ocean Surface Currents Using Complex and Real-Vector Methods. J. Atmos. Oceanic Technol., 15, 927–941, doi: 10.1175/1520-0426(1998)015<0927:EOFAOO>2.0.CO;2, 1998.

465 Kamph, J. and Chapman, P.: Upwelling systems of the world: a scientific journey to the most productive marine ecosystems. Springer, Berlin, 425 pp, 2016.

Kilian, R.andLamy, F.: A review of Glacial and Holocene paleoclimate records from southernmost Patagonia (49–55°S). Quaternary Science Reviews, 53(C), 1–23. https://doi.org/10.1016/j.quascirev.2012.07.017, 2012.

Marcotte, D.:Cokrigeage with matlab, Computers and Geosciences, 17(9), 1265-1280, doi:10.1016/0098-
470 3004(91)90028-C, 1991.

Montero, P., Daneri, G., Cuevas, L. A., González, H. E., Jacob, B., Lizárraga, L., and Menschel, E.: Productivity cycles in the coastal upwelling area off Concepción: The importance of diatoms and bacterioplankton in the organic carbon flux. Progress in Oceanography, 75(3), 518–530. https://doi.org/10.1016/j.pocean.2007.08.013, 2007.

475 Montero, P., Pérez-Santos, I., Daneri, G., Gutiérrez, M., Igor, G., Seguel, R., Crawford, D., and Duncan, P.: A winter dinoflagellate bloom drives high rates of primary production in a Patagonian fjord ecosystem, Estuar. Coast. ShelfSci., 199, 105-116, 2017.

Orlanski, I.: A rational subdivision of scales for atmospheric processes. Bulletin of the American Meteorological Society, 56: 527-530, 1975.

480 Pérez-Santos, I., Schneider, W., Sobarzo, M., Montoya-Sánchez, R., Valle-Levinson, A., and Garcés-Vargas, J.: Surface wind variability and its implications for the Yucatan basin-Caribbean Sea dynamics. Journal of Geophysical Research, 115 (C10), C10052. https://doi.org/10.1029/2010JC006292, 2010.

Pickett, M. H. and Paduan J. D.: Ekman transport and pumping in the California Current based on the U.S. Navy's high resolution atmospheric model (COAMPS), J. Geophys. Res., 108(C10), 3327, doi:10.1029/2003JC001902,
485 2003.

Piolle, J. F. and Bentamy, A.: Mean Wind Fields (MWF product), User Manual, QuikSCAT, CERSAT, Plouzané, 42pp, 2002.

Rahn, D. and Garreaud, R.: A synoptic climatology of the near-surface wind along the west coast of South America. Int. J. Climatol.1-13, 2013.

490 Ray, P.S.: Mesoscale Meteorology and Forecasting. American Meteorological Society, Boston, MA, 793 pp, 1986.

Ross, L., Valle-Levinson, A., Pérez-Santos, I., Tapia, F.,and Schneider, W.: Baroclinic annular variability of internal motions in a Patagonian fjord. Journal of Geophysical Research: Oceans, 120, 5668– 5685. https://doi.org/10.1002/2015JC011264, 2015.

Rykaczewski, R. R. and Checkley, D.M.: Influence of ocean winds on the pelagic ecosystem in upwelling regions. PNAS, 105-6, 1965–1970, 2008.

Schneider, W., Donoso, D., Garcés-Vargas, J., and Escribano, R.: Water-column cooling and sea surface salinity increase in the upwelling region off central-south Chile driven by a poleward displacement of the South Pacific High. Progress in Oceanography, 151, 38–48. https://doi.org/10.1016/j.pocean.2016.11.004, 2017.

Smith, R. L.: Upwelling, Oceanogr, Mar. Biol. Annu. Rev. 6,11-46, 1968.

Sobarzo, M. and Djurfeldt, L.: Coastal upwelling process on a continental shelf limited by submarine canyons, Concepción, central Chile, J. Geophys. Res., 109, C12012, doi:10.1029/2004JC002350, 2004.

Sobarzo, M., Bravo, L., Donoso, D., Garcés-Vargas, J., and Schneider, W.: Coastal upwelling and seasonal cycles that influence the water column over the continental shelf off central Chile, Progress in Oceanography 75, 363–382, 2007.

Stewart, R. H.: Introduction to physical oceanography, Spring 2002 Edition, Department of Oceanography, Texas A and M University, 350pp, 2002.

Talley, L.D., Pickard, G.L., Emery, W.J., and Swift, J.H.: Descriptive physical oceanography, an introduction. Six edition, Academic press, Elsevier, 1-983, 2011.

Thiel, M. et al.: The Humboldt Current system of northern and central Chile. Oceanography and Marine Biology: An Annual Review, 45, 195-344 © R. N. Gibson, R. J. A. Atkinson, and J. D. M. Gordon, Editors Taylor and Francis, 2007.

Thompson, D. W. J.and Barnes, E. A.: Periodic variability in the large-scale southern hemisphere atmospheric circulation, Science, 343, 641–645, 2014.

Thompson, D. W. J.and Woodworth J. D.: Barotropic and baroclinic annular variability in the southern hemisphere, J. Atmos. Sci., 71, 1480–1493, doi:10.1175/JAS-D-13-0185.1, 2014.

Tomasz, N.: Chapter Two - El Niño/Southern Oscillation and Selected Environmental Consequences, Advances in Geophysics, Elsevier, Volume 55, Pp 77-122, 2014.

Tomczak, M. and Godfrey, J. S.: Regional Oceanography: An Introduction, 422 pp, Pergamon, 1994.

Torrence, C.and Compo, G. P.: A Practical Guide to Wavelet Analysis, Bull. Amer. Meteor. Soc., 79, 61–78, doi: 10.1175/1520-0477(1998)079<0061:APGTWA>2.0.CO;2, 1998.

Yelland, M.and Taylor, P.K.: Wind Stress Measurements from the Open Ocean, J. Phys. Oceanogr., 26, 541–558, doi: 10.1175/1520-0485(1996)026<0541:WSMFTO>2.0.CO; 2, 1996.

Ocean Sci. Discuss., https://doi.org/10.5194/os-2018-119
Manuscript under review for journal Ocean Sci.
Discussion started: 16 November 2018

Figure captions

Figure 1. Long term mean of daily surface wind from (**a**) QuikSCAT (1999-2009), and (**b**) ASCAT (2007-2016). Black line: standard deviations from daily data. Color bar: surface wind magnitude.

Figure 2. Eastern Austral Pacific Ocean, 1999 to 2015: normalized eigenvector patterns, from QuikSCAT (**a**, **b**), and (**c**), and ASCAT; surface winds (**d**, **e**, and **f**).

Figure 3. (**a**, **d**, **g**) Normalized time series of the time-dependent coefficient (black lines), with 30 day, low pass filtered time series (solid red lines). (**b**, **e**, **h**) Global wavelet spectra (black solid lines) with 95% confidence interval (red dashed lines), and (**c**, **f**, **i**) long term monthly mean of EOF modes from surface winds daily data on QuikSCAT from 1999 to 2009: mode 1 (**a**, **b**, **c**), mode 2 (**d**, **e**, **f**), mode 3 (**g**, **h**, **i**).

Figure 3. Continued. (**j**, **m**, **p**) Normalized time series of the time-dependent coefficient (black lines) with 30day, low pass filtered time series (solid red lines). (**k**, **n**, **q**) Global wavelet spectra (black solid lines) with 95% confidence interval (red dashed lines) and (**l**, **o**, **r**) long term, monthly mean of EOF modes from surface winds daily data on ASCAT from 2007 to 2015: mode 1 (**j**, **k**, **l**), mode 2 (**m**, **n**, **o**), mode 3 (**p**, **q**, **r**).

Figure 4. Snapshots of surface winds representing EOF eigenvector spatial structures for mode 1 (**a**, **b**), mode 2 (**c**, **d**), and mode 3 (**e** and **f**). Surface wind and atmospheric pressure data were obtained from ERA-Interim product.

Figure 5. Morlet wavelet power spectrum applied to the three series of the empirical orthogonal function time-dependent coefficient from QuikSCAT (**a**, **c**, **e**), and from ASCAT (**b**, **d**, **f**).The fine contour lines enclose regions of confidence levels greater than 95% for a red noise process with a lag 1 coefficient between 0.37 and 0.70, and the thick contour lines indicate the cone of influence. The color bar relates colors to the power spectrum.

Figure 6. Long term mean of daily surface wind stress (black arrows), Ekman transport (red arrows), and Ekman pumping (color bars) from (**a**) QuikSCAT (1999-2009), (**b**) ASCAT (2007-2016). The black lines represent the zero value of Ekman pumping, where a positive number is a region favorable to upwelling and negative to downwelling. The black dots in (**a**) represented the positions of time series shown in Fig. 7.

Figure 7. Quantification of the cross-shore transport using satellite winds products (QuikSCAT and ASCAT) from the north, center and south time series (see Fig. 6 (**a**) for the position), for 1999-2015. (**a**, **d**, **g**) represent the long term daily mean, (**b**, **e**, **h**) the long term monthly mean, and (**c**, **f**, **i**) cumulative Ekman transport, pumping, and total transport. The total transport is the sum of the Ekman transport and pumping. The positive/negative values of transport indicate upwelling/downwelling conditions.

Figure 8. Examples to shows the ocean response to Ekman transport and pumping along the northern coast of Patagonia. Daily images of the wind stress: Ekman transport and pumping from ASCAT wind product (**a**, **d**, g); sea surface temperature (**b**, **e**, **h**), and chlorophyll-a (**c**, **f**, **i**), from MODIS-Aqua.

Figure 9. Surface air temperature and net solar radiation long term hourly means, and histogram of the maximum surface air temperature, from the Puyuhuapi Fjord oceanographic buoy (**a**, **c**, **e**), and meteorological station (**b**, **d**, **f**), for2011-2017. The gray shaded area in (**e** and **f**) shows the times of the second air temperature maxima.

Figure 10. Time series of (**a**) the maximum surface air temperature, (**b**) the histogram, and (**c**) long term monthly mean, for 2011-2017. Data from the Puyuhuapi Fjord oceanographic buoy and meteorological station.

Ocean Sci. Discuss., https://doi.org/10.5194/os-2018-119
Manuscript under review for journal Ocean Sci.
Discussion started: 16 November 2018

Figure 11. Hourly air temperature, atmospheric pressure, and wind speed, from the Puyuhuapi Fjord oceanographic buoy (**a**), and surface winds, atmospheric pressure and surface air temperature from ERA-interim product (**b**) – (**g**), during April 2011.

Figure 12. Hourly data of air temperature, atmospheric pressure, and wind speed from the Puyuhuapi Fjord oceanographic buoy (a), and surface winds, atmospheric pressure and surface air temperature from ERA-interim product (**b**) – (**g**), during July 2012.

Figure 13. A conceptual model of the "Night-time heat wave event" in the Eastern Austral Pacific Ocean. (**a**) The initial condition, where a low atmospheric pressure system with cold air and a high atmospheric pressure system with warm air are regionally present, although separate; (**b**) the low atmospheric pressure system moves northward and encounters the high atmospheric pressure system, advecting warm air to Patagonia.

Ocean Sci. Discuss., https://doi.org/10.5194/os-2018-119
Manuscript under review for journal Ocean Sci.
Discussion started: 16 November 2018

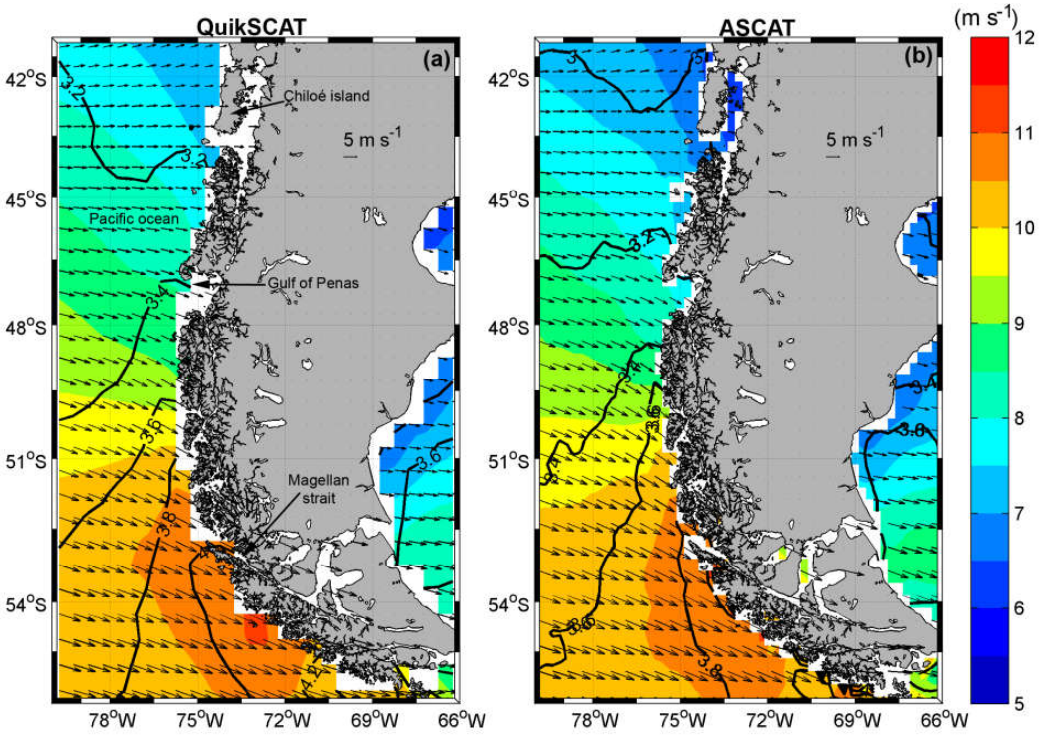

Figure 1. Long term mean of daily surface wind from (**a**) QuikSCAT (1999-2009), and (**b**) ASCAT (2007-2016). Black line: standard deviations from daily data. Color bar: surface wind magnitude.

Ocean Sci. Discuss., https://doi.org/10.5194/os-2018-119
Manuscript under review for journal Ocean Sci.
Discussion started: 16 November 2018

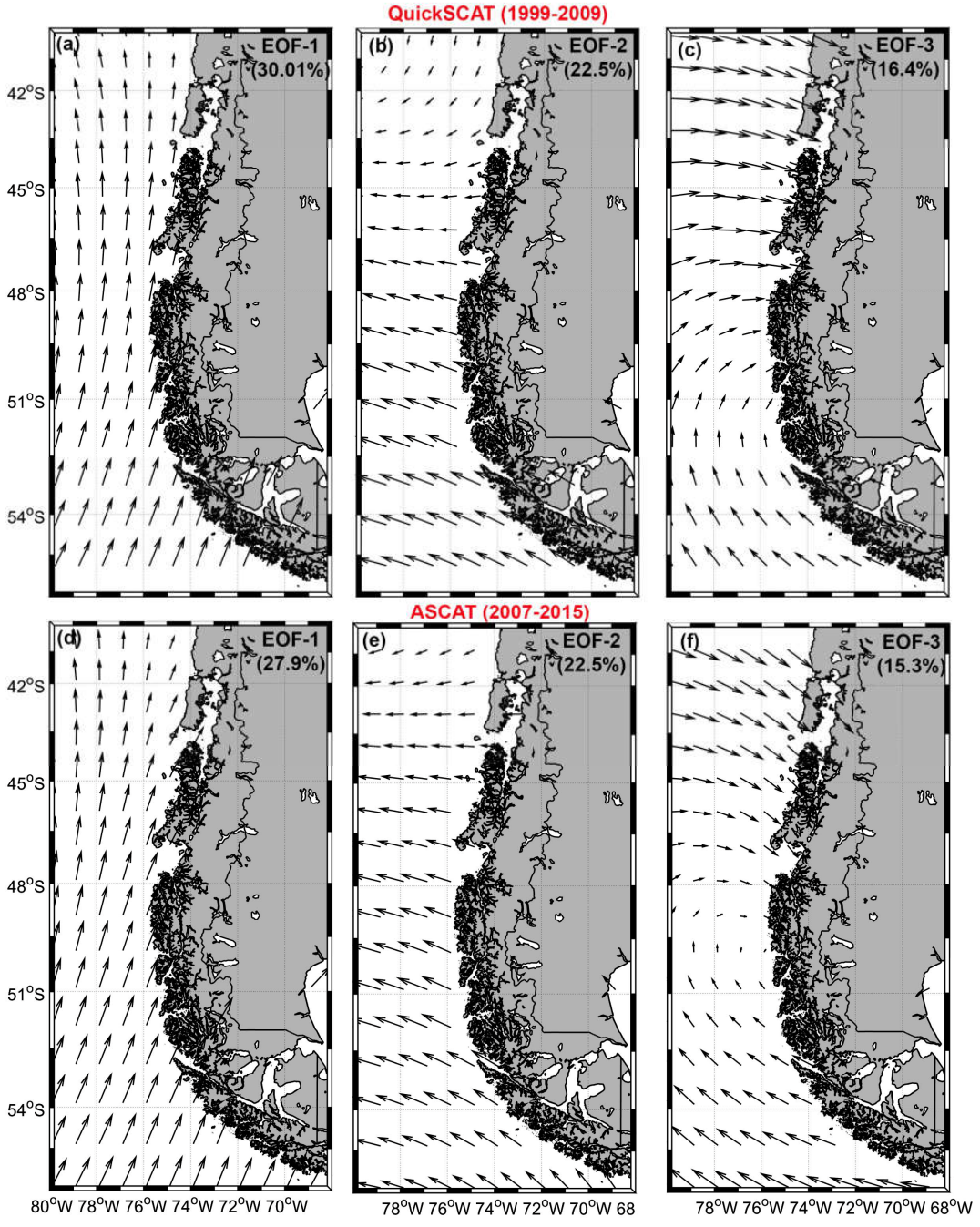

Figure 2. Eastern Austral Pacific Ocean, 1999 to 2015: normalized eigenvector patterns, from QuikSCAT (**a**, **b**), and (**c**), and ASCAT; surface winds (**d**, **e**, and **f**).

Ocean Sci. Discuss., https://doi.org/10.5194/os-2018-119
Manuscript under review for journal Ocean Sci.
Discussion started: 16 November 2018

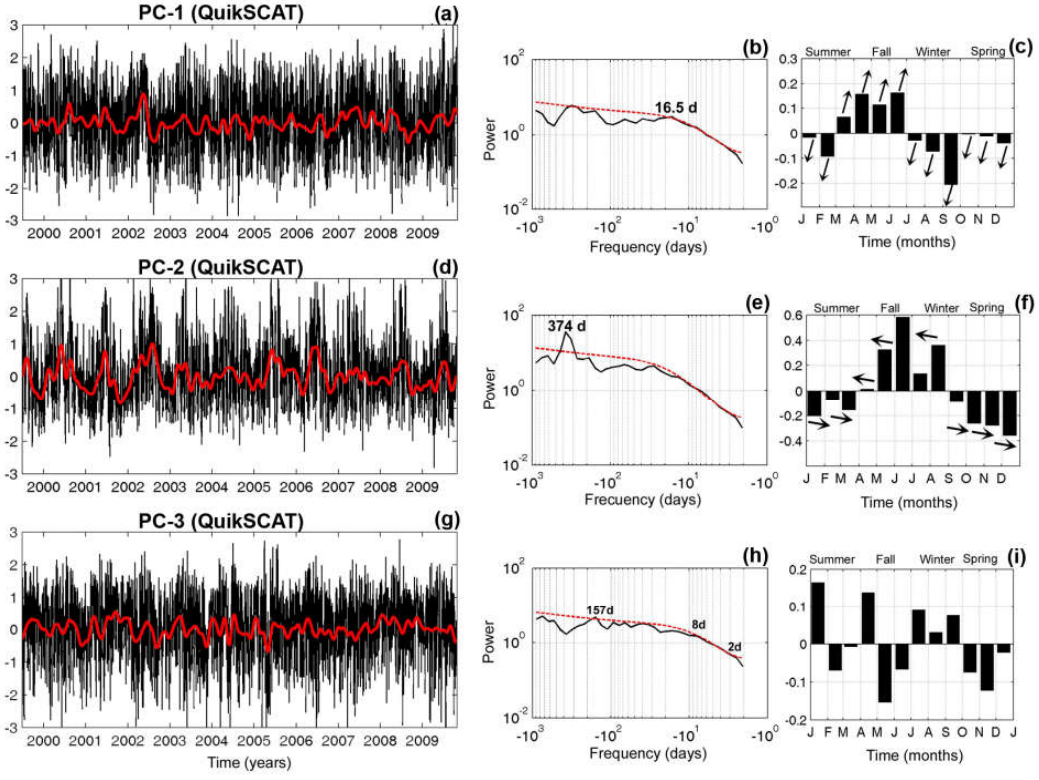

580

Figure 3. (**a**, **d**, **g**) Normalized time series of the time-dependent coefficient (black lines), with 30 day, low pass filtered time series (solid red lines). (**b**, **e**, **h**) Global wavelet spectra (black solid lines) with 95% confidence interval (red dashed lines), and (**c**, **f**, **i**) long term monthly mean of EOF modes from surface winds daily data on QuikSCAT from 1999 to 2009: mode 1 (**a**, **b**, **c**), mode 2 (**d**, **e**, **f**), mode 3 (**g**, **h**, **i**).

585

Ocean Sci. Discuss., https://doi.org/10.5194/os-2018-119
Manuscript under review for journal Ocean Sci.
Discussion started: 16 November 2018

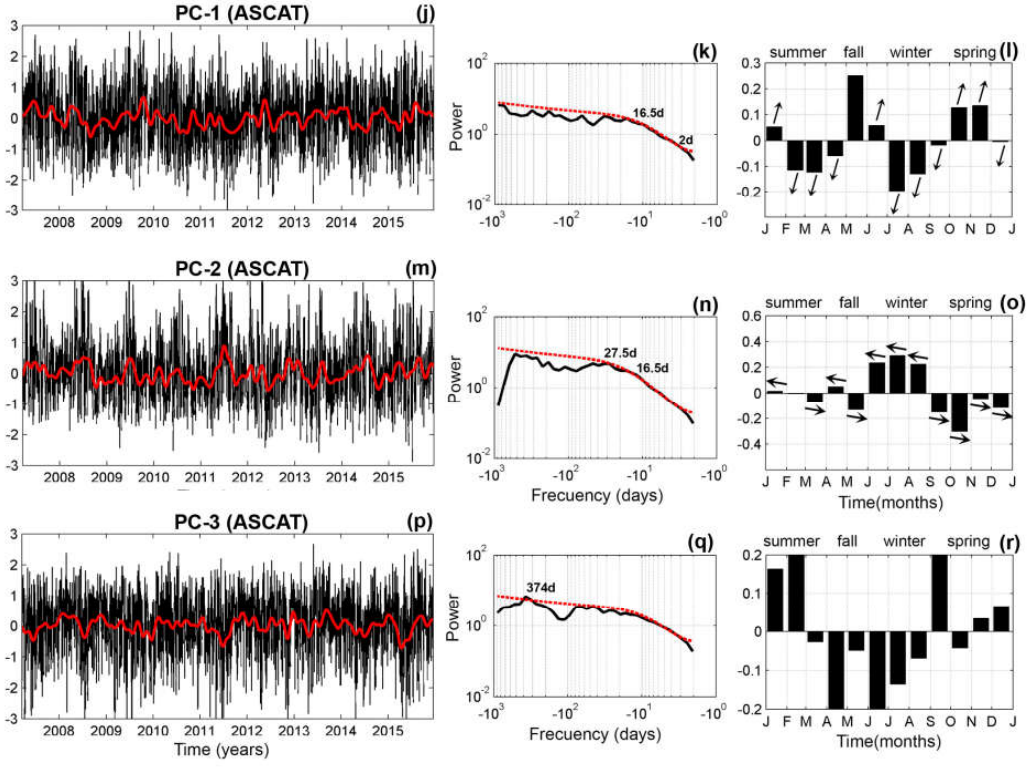

Figure 3. Continued. (**j**, **m**, **p**) Normalized time series of the time-dependent coefficient (black lines) with 30day, low pass filtered time series (solid red lines). (**k**, **n**, **q**) Global wavelet spectra (black solid lines) with 95% confidence interval (red dashed lines) and (**l**, **o**, **r**) long term, monthly mean of EOF modes from surface winds daily data on ASCAT from 2007 to 2015: mode 1 (**j**, **k**, **l**), mode 2 (**m**, **n**, **o**), mode 3 (**p**, **q**, **r**).

Ocean Sci. Discuss., https://doi.org/10.5194/os-2018-119
Manuscript under review for journal Ocean Sci.
Discussion started: 16 November 2018

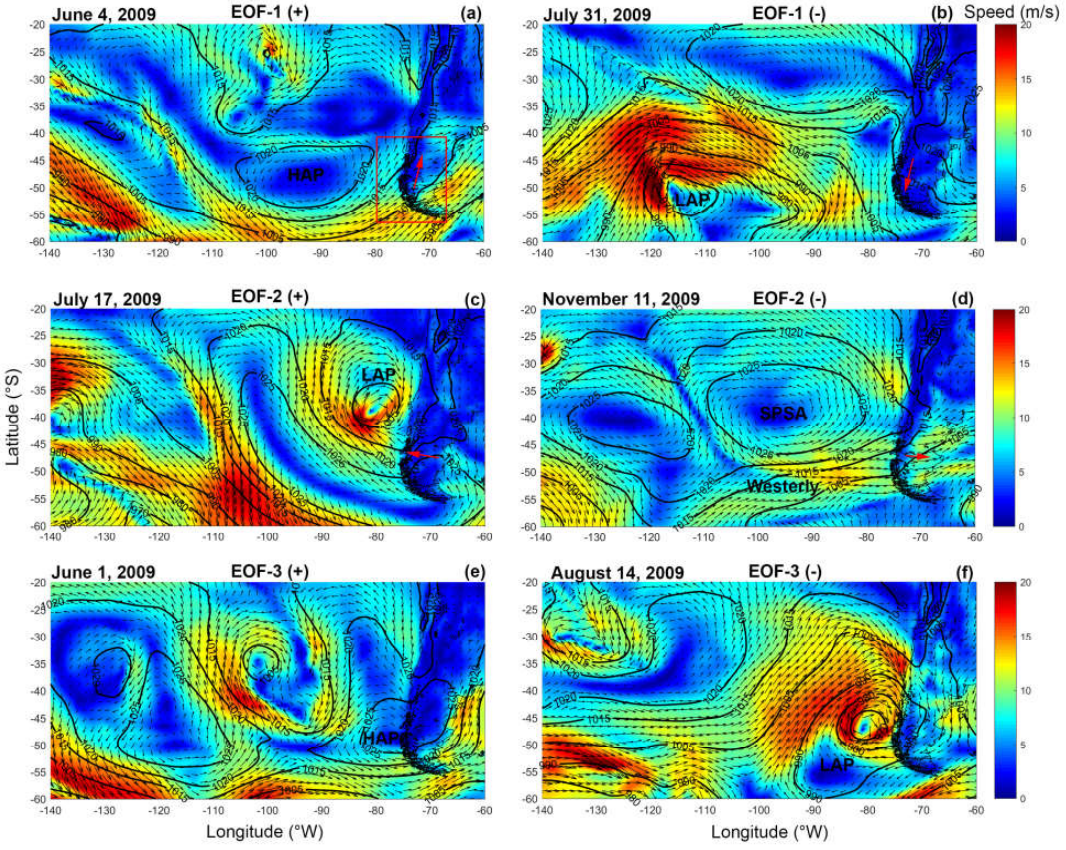

Figure 4. Snapshots of surface winds representing EOF eigenvector spatial structures for mode 1 (**a**, **b**), mode 2 (**c**, **d**), and mode 3 (**e** and **f**). Surface wind and atmospheric pressure data were obtained from ERA-Interim product.

595

Ocean Sci. Discuss., https://doi.org/10.5194/os-2018-119
Manuscript under review for journal Ocean Sci.
Discussion started: 16 November 2018

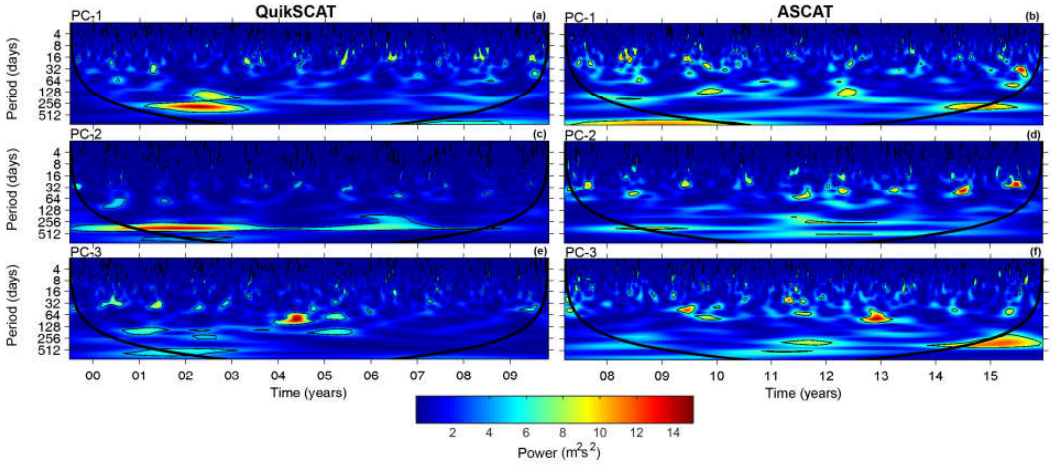

Figure 5. Morlet wavelet power spectrum applied to the three series of the empirical orthogonal function time-dependent coefficient from QuikSCAT (**a**, **c**, **e**), and from ASCAT (**b**, **d**, **f**).The fine contour lines enclose regions of confidence levels greater than 95% for a red noise process with a lag 1 coefficient between 0.37 and 0.70, and the thick contour lines indicate the cone of influence. The color bar relates colors to the power spectrum.

Ocean Sci. Discuss., https://doi.org/10.5194/os-2018-119
Manuscript under review for journal Ocean Sci.
Discussion started: 16 November 2018

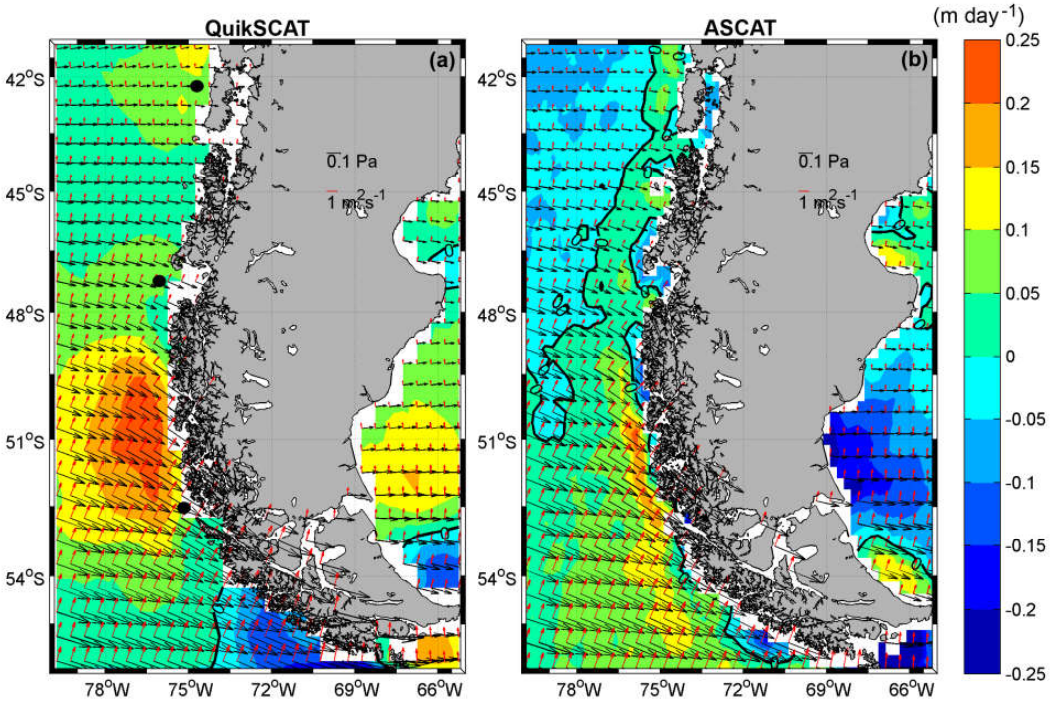

Figure 6. Long term mean of daily surface wind stress (black arrows), Ekman transport (red arrows), and Ekman pumping (color bars) from (**a**) QuikSCAT (1999-2009), (**b**) ASCAT (2007-2016). The black lines represent the zero value of Ekman pumping, where a positive number is a region favorable to upwelling and negative to downwelling. The black dots in (**a**) represented the positions of time series shown in Fig. 7.

Ocean Sci. Discuss., https://doi.org/10.5194/os-2018-119
Manuscript under review for journal Ocean Sci.
Discussion started: 16 November 2018

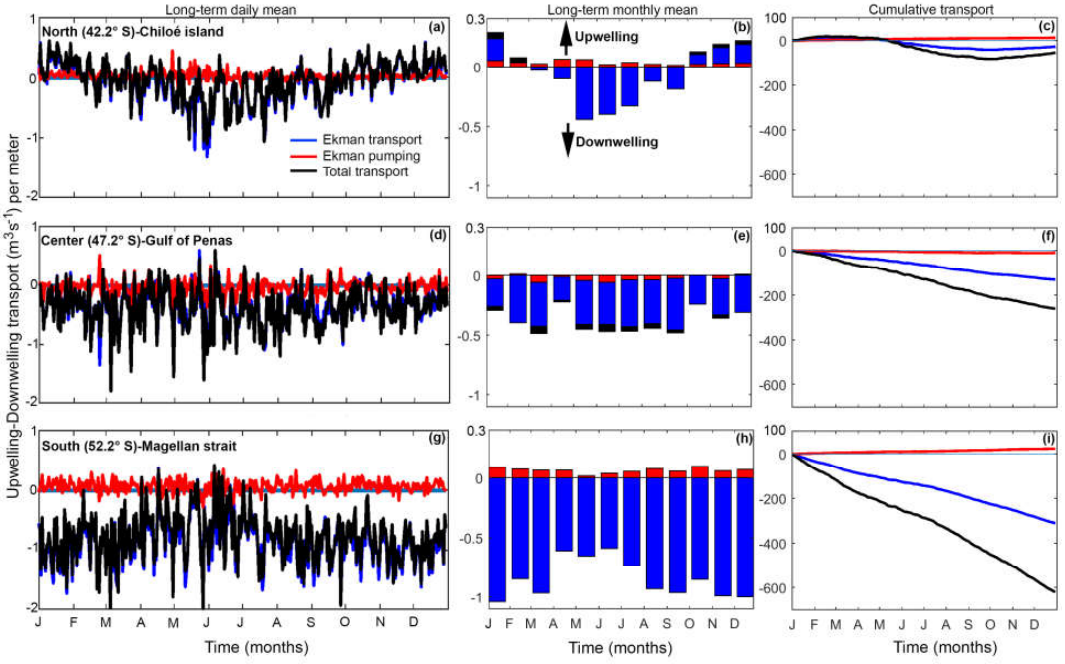

Figure 7. Quantification of the cross-shore transport using satellite winds products (QuikSCAT and ASCAT) from the north, center and south time series (see Fig. 6 (**a**) for the position), for 1999-2015. (**a**, **d**, **g**) represent the long term daily mean, (**b**, **e**, **h**) the long term monthly mean, and (**c**, **f**, **i**) cumulative Ekman transport, pumping, and total transport. The total transport is the sum of the Ekman transport and pumping. The positive/negative values of transport indicate upwelling/downwelling conditions.

Ocean Sci. Discuss., https://doi.org/10.5194/os-2018-119
Manuscript under review for journal Ocean Sci.
Discussion started: 16 November 2018

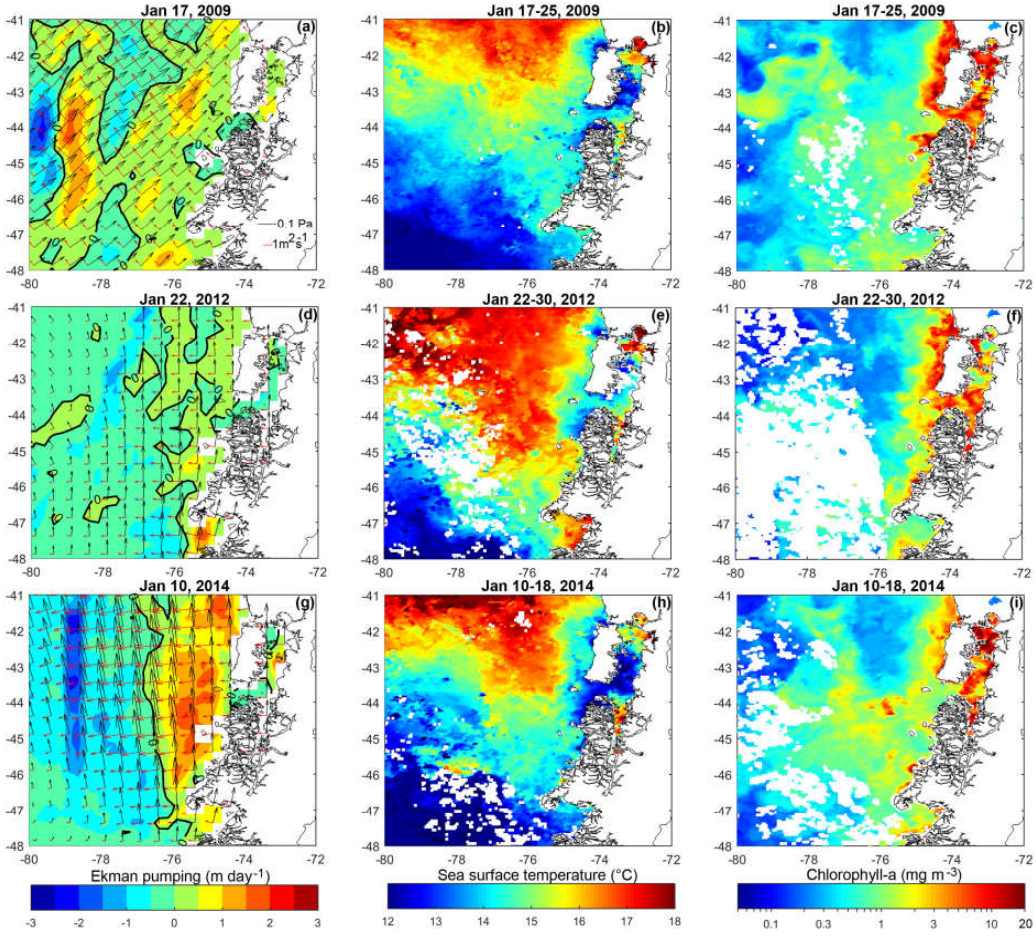

Figure 8. Examples to shows the ocean response to Ekman transport and pumping along the northern coast of Patagonia. Daily images of the wind stress: Ekman transport and pumping from ASCAT wind product (**a**, **d**, g); sea surface temperature (**b**, **e**, **h**), and chlorophyll-a (**c**, **f**, **i**), from MODIS-Aqua.

Ocean Sci. Discuss., https://doi.org/10.5194/os-2018-119
Manuscript under review for journal Ocean Sci.
Discussion started: 16 November 2018

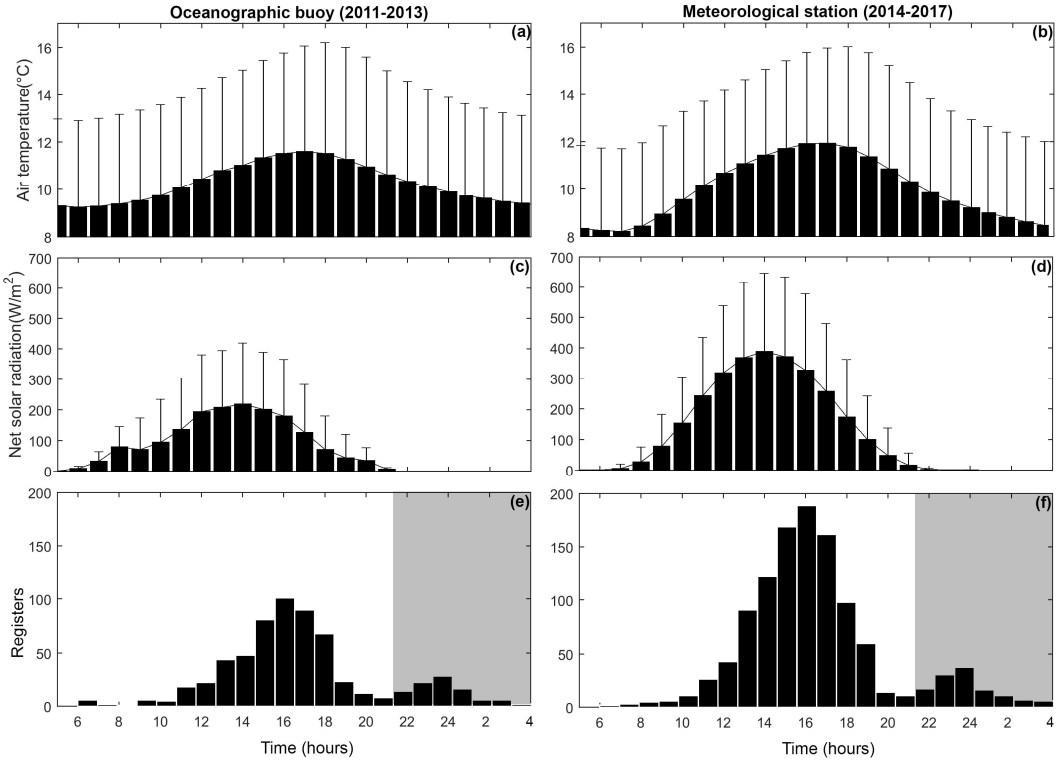

Figure 9. Surface air temperature and net solar radiation long term hourly means, and histogram of the maximum surface air temperature, from the Puyuhuapi Fjord oceanographic buoy (**a**, **c**, **e**), and meteorological station (**b**, **d**, **f**), for2011-2017. The gray shaded area in (**e** and **f**) shows the times of the second air temperature maxima.

Ocean Sci. Discuss., https://doi.org/10.5194/os-2018-119
Manuscript under review for journal Ocean Sci.
Discussion started: 16 November 2018

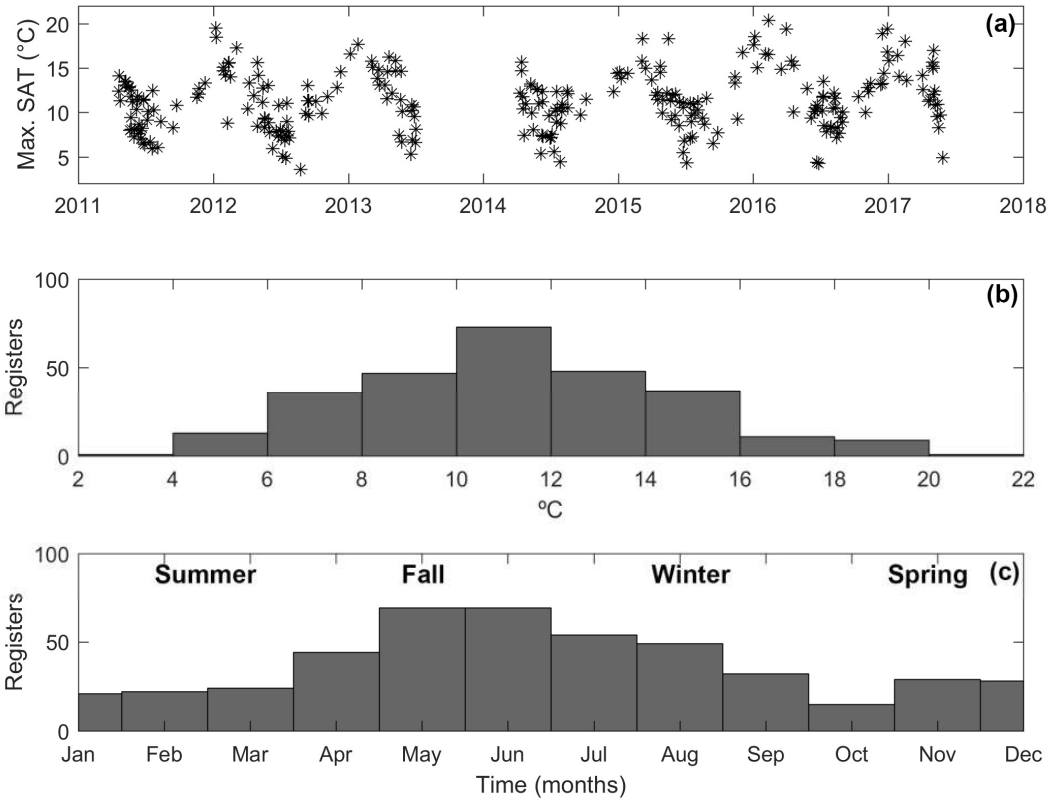

Figure 10. Time series of (**a**) the maximum surface air temperature, (**b**) the histogram, and (**c**) long term monthly mean, for 2011-2017. Data from the Puyuhuapi Fjord oceanographic buoy and meteorological station.

Ocean Sci. Discuss., https://doi.org/10.5194/os-2018-119
Manuscript under review for journal Ocean Sci.
Discussion started: 16 November 2018

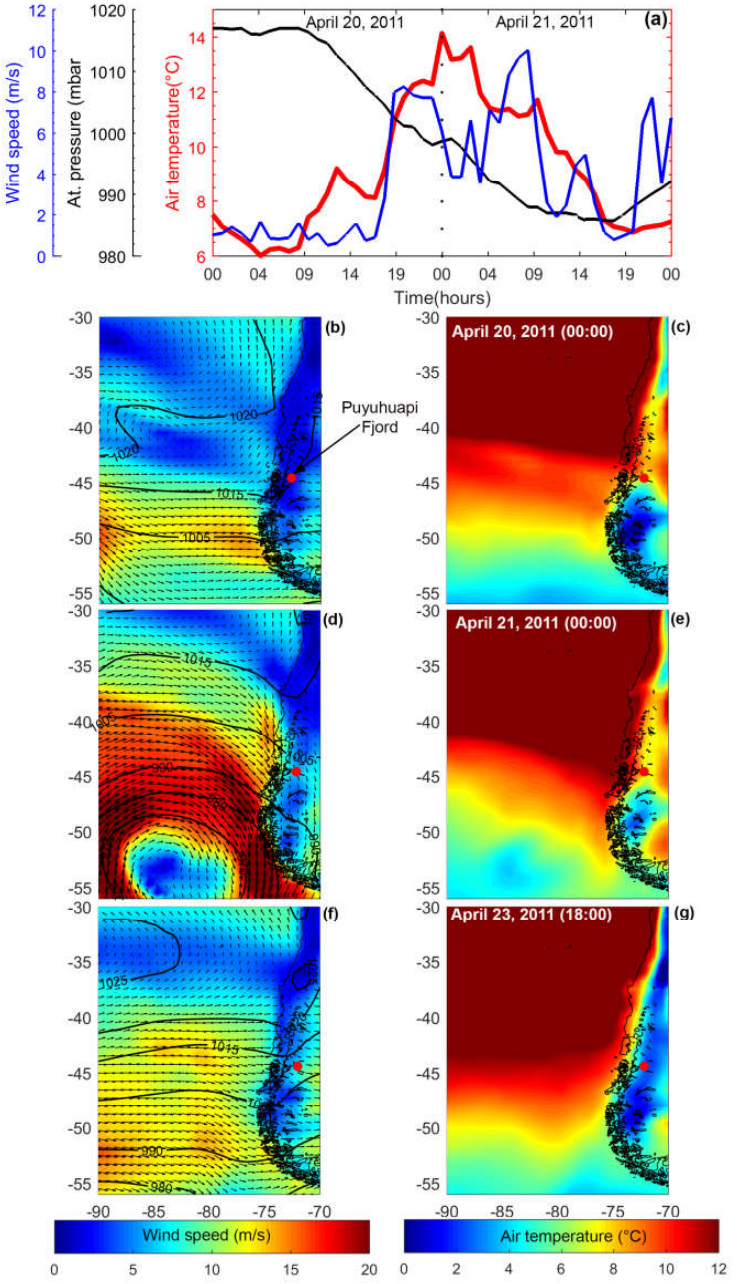

Figure 11. Hourly air temperature, atmospheric pressure, and wind speed, from the Puyuhuapi Fjord oceanographic buoy (**a**), and surface winds, atmospheric pressure and surface air temperature from ERA-interim product (**b**) – (**g**), during April 2011.

Ocean Sci. Discuss., https://doi.org/10.5194/os-2018-119
Manuscript under review for journal Ocean Sci.
Discussion started: 16 November 2018

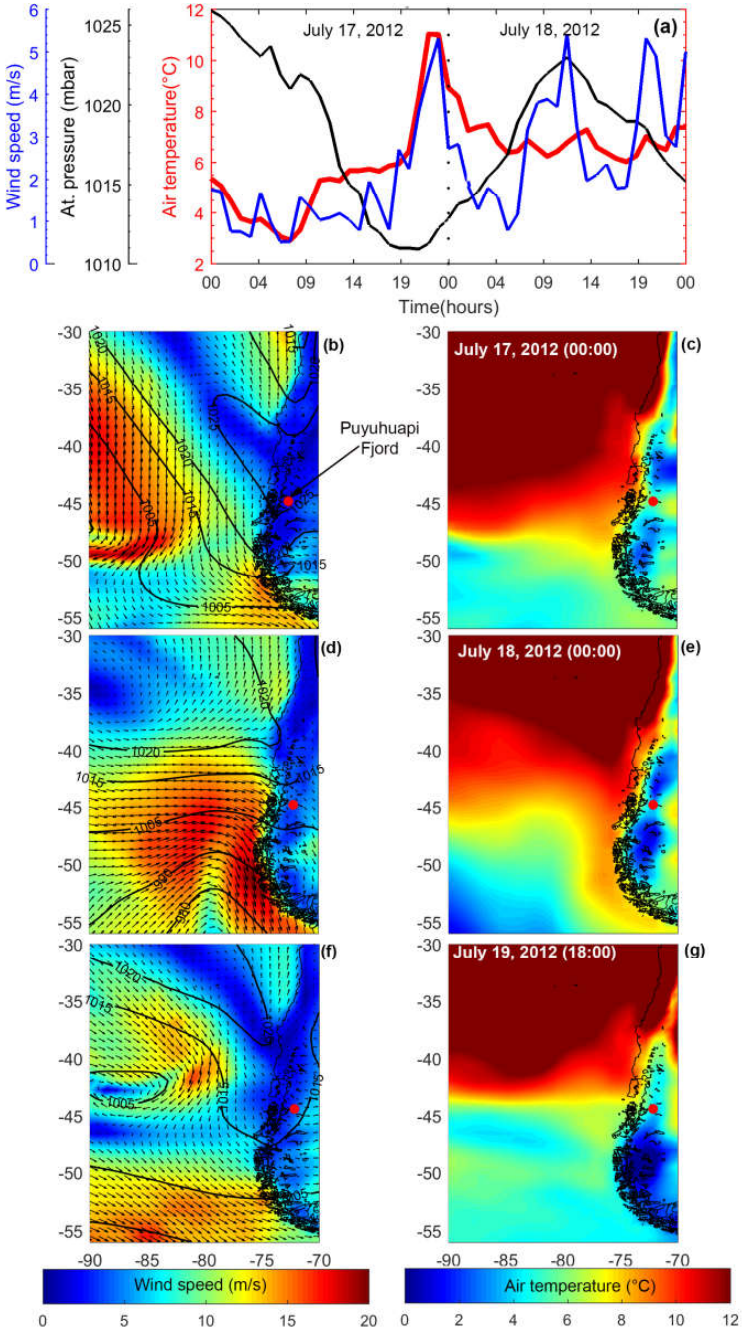

Figure 12. Hourly data of air temperature, atmospheric pressure, and wind speed from the Puyuhuapi Fjord oceanographic buoy (a), and surface winds, atmospheric pressure and surface air temperature from ERA-interim product (**b**) – (**g**), during July 2012.

Ocean Sci. Discuss., https://doi.org/10.5194/os-2018-119
Manuscript under review for journal Ocean Sci.
Discussion started: 16 November 2018

Ocean Science
Discussions
Open Access
EGU

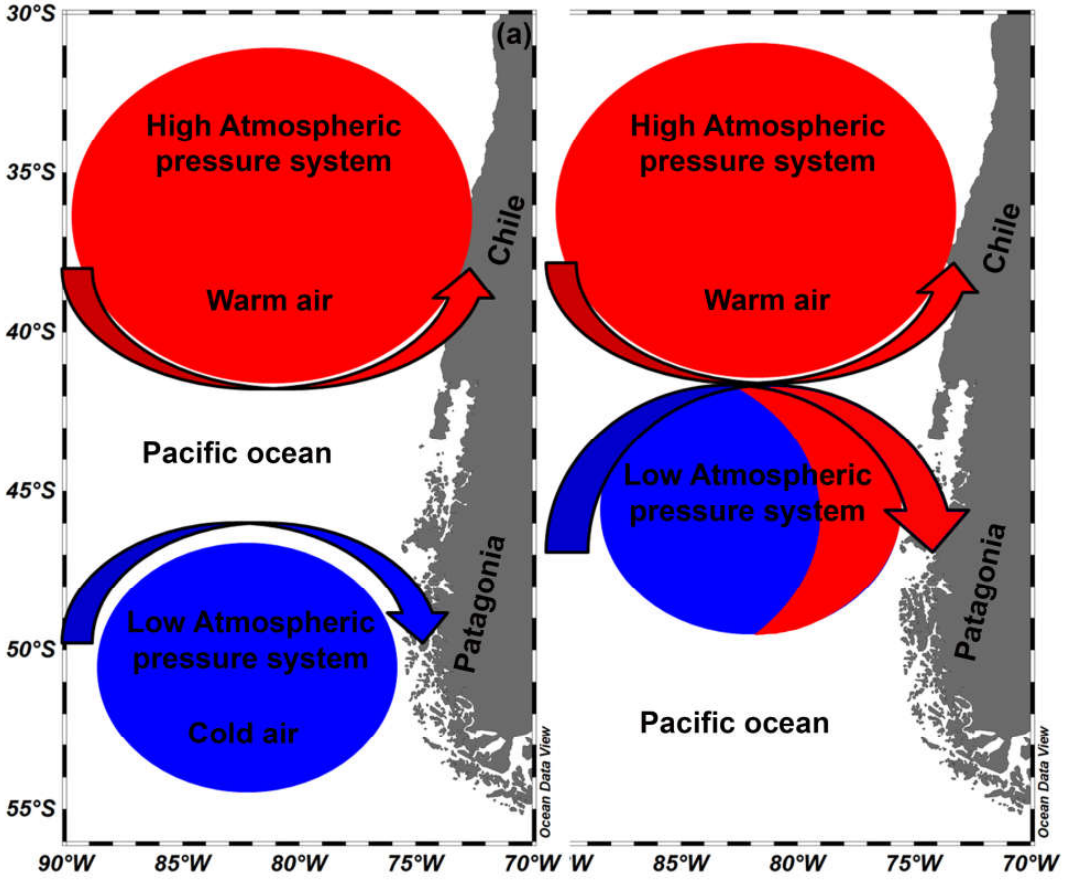

Figure 13. A conceptual model of the "Night-time heat wave event" in the Eastern Austral Pacific Ocean. (**a**) The initial condition, where a low atmospheric pressure system with cold air and a high atmospheric pressure system with warm air are regionally present, although separate; (**b**) the low atmospheric pressure system moves northward and encounters the high atmospheric pressure system, advecting warm air to Patagonia.